Polarized light scattering by hexagonal ice crystals: theory

Qiming Cai and Kuo-Nan Liou

A scattering model involving complete polarization information for arbitrarily oriented hexagonal columns and plates is developed on the basis of the ray tracing principle which includes contributions from geometric reflection and refraction and Fraunhofer diffraction. We present a traceable and analytic procedure for computation of the scattered electric field and the associated path length for rays undergoing external reflection, two refractions, and internal reflections. We also derive an analytic expression for the scattering electric field in the limit of Fraunhofer diffraction due to an oblique hexagonal aperture. Moreover the theoretical foundation and procedures are further developed for computation of the scattering phase matrix containing 16 elements for randomly oriented hexagonal crystals. Results of the six independent scattering phase matrix elements for randomly oriented large columns and small plates, having length-to-radius ratios of 300/60 and 8/10 μm, respectively, reveal a number of interesting and pronounced features in various regions of the scattering angle when a visible wavelength is utilized in the ray tracing program. Comparisons of the computed scattering phase function, degree of linear polarization, and depolarization ratio for randomly oriented columns and plates with the experimental scattering data obtained by Sassen and Liou for small plates are carried out. We show that the present theoretical results within the context of the geometric optics are in general agreement with the laboratory data, especially for the depolarization ratio.

I. Introduction

Angular scattering and polarization behaviors of atmospheric ice crystals are fundamental to development of remote sounding techniques for the inference of cloud compositions. They also influence the radiation budget of the earth's atmosphere containing ice clouds and consequently affect the weather and climate of the earth. Previous theoretical and experimental studies on light scattering by nonspherical ice crystals have been limited to unpolarized cases[1–3] or cases involving two components of linear polarization.[4,5]

In this paper, we wish to develop a scattering model for hexagonal ice crystals including the complete polarization information based on the geometric ray tracing principle. In Sec. II we first describe the basic coordinate system with respect to the hexagonal ice crystal and incident electric vector. We then present the electric field vectors and the corresponding direction cosines for rays undergoing external reflection, two refractions, and internal reflections. Subsequently we discuss phase shifts of these rays due to different optical paths and derive the total scattered electric vector due to geometric reflection and refraction. In Sec. III we provide a discussion on diffraction in the Fraunhofer limit for the far field and derive an analytic expression for wave disturbance of light beams produced by an aperture which is a projection of a hexagonal crystal on the plane normal to an oblique incident ray. In Sec. IV we present equations for computation of the 4×4 scattering phase matrix for randomly oriented ice crystals in 2- and 3-D space based on results derived from Secs. II and III. Computational results for randomly oriented hexagonal columns and plates using a visible wavelength are given in Sec. V. In this section we also compare the phase function, degree of linear polarization, and depolarization ratio computed from the present theory for columns and plates with those obtained from the laboratory scattering and cloud physics experiments. Finally concluding remarks are in Sec. VI.

II. Geometric Ray Tracing Analyses

The laws of geometrical optics can be applied under the condition that the size of a hexagonal ice crystal is much larger than the wavelength of light. In this case, a light beam may be thought of as consisting of a bundle of separate rays which hits the ice crystal so that the width of the light beam is much larger than the wavelength and yet small compared with crystal size. Every ray hitting the crystal undergoes reflection, refraction, and diffraction on the hexagonal ice crystal surfaces and pursues its own specific path. In the course of reflection, refraction, and diffraction the rays emerge from various directions and have different amplitudes and

The authors are with University of Utah, Meteorology Department, Salt Lake City, Utah 84112.
Received 4 March 1982.
0003-6935/82/193569-12$01.00/0.

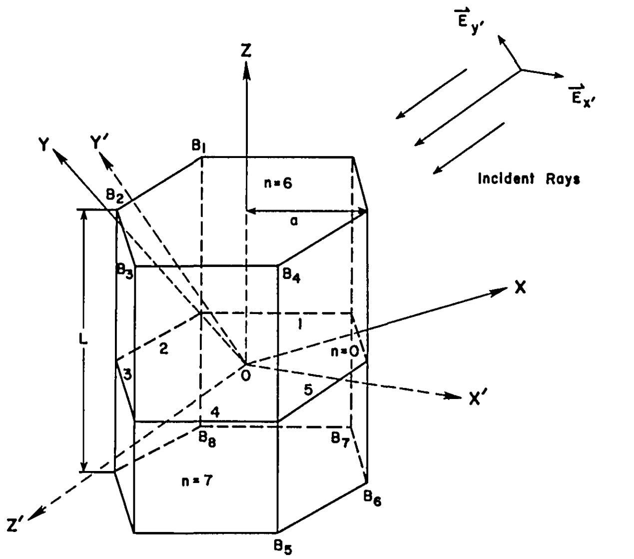

Fig. 1. Geometry of the orientation of a hexagon with respect to the incident electric vector of a geometric ray. The incident electric vector is defined in the $OX'Y'Z'$ coordinate, whereas orientation of the hexagon is fixed in the $OXYZ$ coordinate. Points B_i ($i = 1, 8$) denote the position of the eight vertices of the hexagon corresponding to the aperture cross section for diffraction calculations (also see Fig. 4).

Table I. Definitions of the Direction Cosines

	X	Y	Z
X'	$\cos\alpha_{11}$	$\cos\alpha_{12}$	$\cos\alpha_{13}$
Y'	$\cos\alpha_{21}$	$\cos\alpha_{22}$	$\cos\alpha_{23}$
Z'	$\cos\alpha_{31}$	$\cos\alpha_{32}$	$\cos\alpha_{33}$

phases. We wish to find the amplitude and phase of the outgoing electric fields due to reflection and refraction as a function of the scattering angle and to consider the phase shift due to the optical path lengths of the rays. We will then sum the electric fields of the rays which have the same scattering angle. Finally diffraction due to a hexagonal ice crystal will be added to obtain a complete scattered electric field.

A. Coordinate Systems

We shall first describe a number of coordinate systems which are pertinent for the geometric ray tracing discussion involving an oriented hexagonal ice crystal in space. There are two series of independent variables with respect to the incident and scattered electric fields and with respect to the position of a hexagon. We define two Cartesian coordinate systems, $OXYZ$ and $OX'Y'Z'$, in such a way that the origin O is placed at the center of the hexagon. The relative orientation of the hexagon is fixed on the $OXYZ$ coordinate system. Let OZ be the vertical axis of the hexagon and OX be perpendicular to one of its side surfaces as illustrated in Fig. 1. Let the coordinate system $OX'Y'Z'$ be associated with the electric field vector so that the axis OZ' is along the incident direction, and axes OX' and OY' represent the directions of two electric field components as shown in Fig. 1. Thus the orientation of a hexagon in space relative to the incident electric vector can be completely expressed by the direction cosines between the six axes of $OXYZ$ and $OX'Y'Z'$ which are listed in Table I.

Only three of the nine direction cosines listed in Table I are independent because of the following six geometric relationships:

$$\sum_{i=1}^{3} \cos^2\alpha_{ij} = 1, \qquad \sum_{j=1}^{3} \cos^2\alpha_{ij} = 1, \qquad i,j = 1, 2, 3. \tag{1}$$

Now let L denote the length of the ice crystal and a the width of the hexagon. The plane equations which describe the eight crystal surfaces in the $OXYZ$ coordinate system may be written in the form

$$\cos\left(\frac{n\pi}{3}\right)x + \sin\left(\frac{n\pi}{3}\right)y - \frac{\sqrt{3}}{2}a = 0, \qquad n = 0, 1, 2, 3, 4, 5,$$

$$\cos[(n-6)\pi]z - \frac{L}{2} = 0, \qquad n = 6, 7. \tag{2}$$

In Eqs. (1) and (2) $n = 0$ denotes the surface perpendicular to the OX axis. The other five side surfaces are successively represented by $n = 1, 2, 3, 4$, and 5, while $n = 6$ and 7 denotes the top and bottom surfaces, respectively. The direction cosines for the normals of the surfaces in the coordinate system $OXYZ$ are given by

$$\left.\begin{aligned} \cos\alpha_n &= \cos\left(\frac{n\pi}{3}\right) \\ \cos\beta_n &= \sin\left(\frac{n\pi}{3}\right) \\ \cos\gamma_n &= 0 \end{aligned}\right\} n = 0, 1, 2, 3, 4, 5, \tag{3}$$

$$\left.\begin{aligned} \cos\alpha_n &= 0 \\ \cos\beta_n &= 0 \\ \cos\gamma_n &= \cos[(n-6)\pi] \end{aligned}\right\} n = 6, 7. \tag{4}$$

Let $E_{x'0}$ and $E_{y'0}$ be two components of the incident electric fields along the OX' and OY' directions which have arbitrary amplitudes and phases. The traveling direction of the ray is along the OZ' axis. Assume that the ray hits the crystal surface n_1 at the point $N_1(x_1,y_1,z_1)$, where $n_1 = 0, 1, 5$, or 6. Let $\mathbf{n}_1$ denote the normal vector of the surface n_1, and its direction is pointing toward space. The three direction cosines relative to the axes OX', OY', and OZ' are denoted by $\cos\xi_1$, $\cos\zeta_1$, and $\cos\eta_1$, which can be obtained by a coordinate transformation from its direction cosines in the $OXYZ$ system into the $OX'Y'Z'$ system in the form

$$\begin{bmatrix} \cos\xi_1 \\ \cos\zeta_1 \\ \cos\eta_1 \end{bmatrix} = \mathbf{A} \begin{bmatrix} \cos\alpha_1 \\ \cos\beta_1 \\ \cos\gamma_1 \end{bmatrix}, \tag{5}$$

where the $\mathbf{A}$ matrix is given by

$$\mathbf{A} = \begin{bmatrix} \cos\alpha_{11} & \cos\alpha_{12} & \cos\alpha_{13} \\ \cos\alpha_{21} & \cos\alpha_{22} & \cos\alpha_{23} \\ \cos\alpha_{31} & \cos\alpha_{32} & \cos\alpha_{33} \end{bmatrix}. \tag{6}$$

The plane denoted by $BO'AO''$, which contains both the normal $\mathbf{n}_1$ and the axis OZ', is the incident plane of the electric vector [see Fig. 2(a)]. It is convenient to define a new rectangular coordinate system $OX_1^iY_1^iZ_1^i$ so that the axis OZ_1^i coincides with OZ', while OX_1^i and OY_1^i are on and perpendicular to the incident plane. The angle between the positive OX_1^i and $\mathbf{n}_1$ is <180° [Fig. 2(a)]. The other two coordinate systems $OX_1^rY_1^rZ_1^r$ and $OX_1^tY_1^tZ_1^t$ in which the coordinate axes OZ_1^r and OZ_1^t are the directions of the first reflected and refracted rays, OX_1^r and OX_1^t are on the incident plane, and OY_1^r and OY_1^t are perpendicular to the incident plane.

B. External Reflection and First Refraction

To obtain the electric fields for rays undergoing external reflection and first refraction, it is necessary to define the two components of the electric fields on and perpendicular to the incident plane so that the Fresnel formulas can be used. Let E_{x1}^i and E_{y1}^i denote the electric field components of the incident ray along the OX_1^i and OY_1^i directions. Through a coordinate transformation from $OX'Y'Z'$ to $OX_1^iY_1^iZ_1^i$ we may write them in a matrix form as

$$\mathbf{E}_1^i = \begin{bmatrix} E_{x1}^i \\ E_{y1}^i \end{bmatrix} = \begin{bmatrix} \cos\phi_1^i & \sin\phi_1^i \\ -\sin\phi_1^i & \cos\phi_1^i \end{bmatrix} \begin{bmatrix} E_{x0}' \\ E_{y0}' \end{bmatrix}, \tag{7}$$

where ϕ_1^i, representing the angle between the axes OX' and OX_1^i, is the angle of the incident plane relative to the axis OX' as shown in Fig. 2. From the geometry we find

$$\cos\phi_1^i = \frac{\cos\xi_1}{\sin\eta_1}, \qquad \sin\phi_1^i = \frac{\cos\zeta_1}{\sin\eta_1}. \tag{8}$$

Note that in Fig. 2(a) η_1 and ξ_1 are given by the arcs $O'AC$ and DC, respectively, and ζ_1 is the angle between $\mathbf{n}_1$ and OY', which is not shown in the figure.

Now we may use the Fresnel formulas to obtain expressions for the reflected and refracted electric fields in matrix forms[6]

$$\mathbf{E}_1^r = \mathbf{R}_1\mathbf{E}_1^i, \quad \mathbf{E}_1^t = \mathbf{T}_1\mathbf{E}_1^i, \tag{9}$$

where

$$\mathbf{E}_1^r = \begin{bmatrix} E_{x1}^r \\ E_{y1}^r \end{bmatrix}, \qquad \mathbf{E}_1^t = \begin{bmatrix} E_{x1}^t \\ E_{y1}^t \end{bmatrix}, \tag{10}$$

$$\mathbf{R}_1 = \begin{bmatrix} R_{x1} & 0 \\ 0 & R_{y1} \end{bmatrix}, \quad \mathbf{T}_1 = \begin{bmatrix} T_{x1} & 0 \\ 0 & T_{y1} \end{bmatrix}. \tag{11}$$

The elements in the matrices E_{x1}^r and E_{y1}^r represent two components of the externally reflected field in the directions of OX_1^r and OY_1^r, E_{x1}^t and E_{y1}^t the corresponding components for the refracted field in the directions of OX_1^t and OY_1^t, R_{x1} and R_{y1} the Fresnel reflection coefficients on and perpendicular to the incident plane, and T_{x1} and T_{y1} the corresponding Fresnel refraction coefficients. On the basis of the relative direction shown in Fig. 2(a), the Fresnel coefficients may be written

$$R_{x1} = -\frac{m_2\cos\tau_1^i - m_1\cos\tau_1^t}{m_2\cos\tau_1^i + m_1\cos\tau_1^t}, \qquad R_{y1} = -\frac{m_1\cos\tau_1^i - m_2\cos\tau_1^t}{m_1\cos\tau_1^i + m_2\cos\tau_1^t},$$
$$T_{x1} = \frac{2m_1\cos\tau_1^i}{m_1\cos\tau_1^t + m_2\cos\tau_1^i}, \qquad T_{y1} = \frac{2m_1\cos\tau_1^i}{m_1\cos\tau_1^i + m_2\cos\tau_1^t}, \tag{12}$$

where m_1 and m_2 are the refractive indices of air and ice, respectively, and τ_1^i and τ_1^t are the incident and refracted angles of the ray. According to reflection and refraction laws in the context of geometrical optics, we find

$$\left.\begin{aligned} \cos\tau_1^i &= -\cos\eta_1 \\ \sin\tau_1^t &= \sin\tau_1^i/m \end{aligned}\right\}, \tag{13}$$

where m is the ratio m_2/m_1. Generally it is a complex number given by $m = m_r + im_i$, where m_r and m_i are the real and imaginary parts of the complex refraction index.

Equations (11) and (12) include not only the information of the amplitude but also the phase of the fields. Consequently Eqs. (9) and (10) describe the complete optical characteristics of one-time reflected and refracted electric fields.

After the magnitude of the electric fields has been obtained, the next problem is to determine the directions of the electric vector and the rays, i.e., the directions of axes OX_1^r, OY_1^r, OZ_1^r, OX_1^t, OY_1^t, and OZ_1^t. These vectors may be determined since the direction cosines of the six axes of the coordinate systems $OX_1^rY_1^rZ_1^r$ and $OX_1^tY_1^tZ_1^t$ relative to $OX_1^iY_1^iZ_1^i$ are

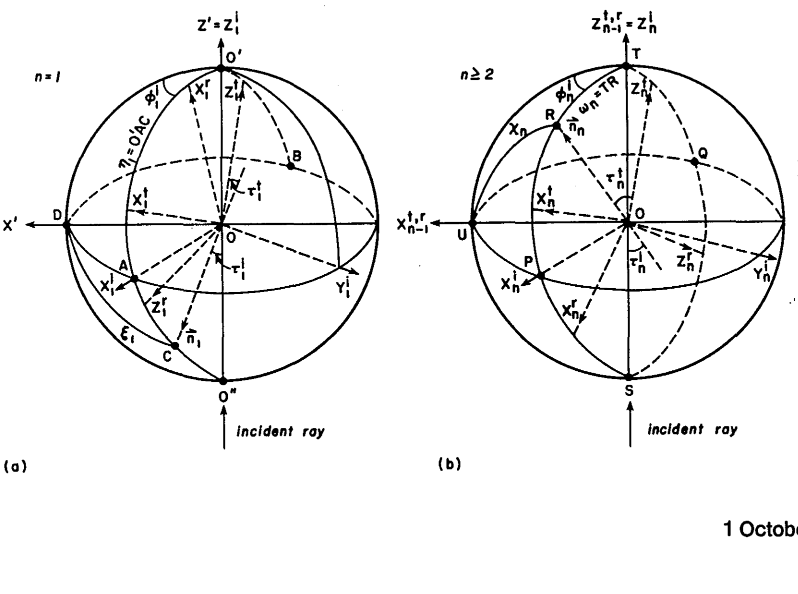

Fig. 2. Geometry defining the incident, reflected, and refracted rays and angles. Figure 2(a) is for external reflection and first refraction ($n = 1$). The incident, reflected, and refracted ray paths are defined on the plane $BO'ACO''$, and $\mathbf{n}_1$ is the normal vector to one of the hexagonal surfaces. Figure 2(b) is for two refractions and internal reflections ($n \geq 2$). The incident ray is now in the hexagon. The incident, internally reflected, and refracted ray paths are defined on the plane $QTRPS$. All the angles and coordinate systems are described in the text.

Table II. Direction Cosines Between $OX_1^rY_1^rZ_1^r$ and $OX_1^tY_1^tZ_1^t$ and $OX_1^iY_1^iZ_1^i$

	X_1^r	Y_1^r	Z_1^r	X_1^t	Y_1^t	Z_1^t
X_1^i	$\cos(2\tau_1^i)$	0	$\sin(2\tau_1^i)$	$\cos(\tau_1^i - \tau_1^t)$	0	$-\sin(\tau_1^i - \tau_1^t)$
Y_1^i	0	−1	0	0	1	0
Z_1^i	$\sin(2\tau_1^i)$	0	$-\cos(2\tau_1^i)$	$\sin(\tau_1^i - \tau_1^t)$	0	$\cos(\tau_1^i - \tau_1^t)$

known. Because the orientation of the incident ray has been given in the coordinate system $OX'Y'Z'$, it would be more convenient to express the direction of the reflected and refracted electric fields in the same system. Referring to Fig. 2(a), the direction cosines of the six axes of the coordinate systems $OX_1^rY_1^rZ_1^r$ and $OX_1^tY_1^tZ_1^t$ with respect to $OX_1^iY_1^iZ_1^i$ are listed in Table II.

Thus the direction cosines of the six axes relative to $OX'Y'Z'$ may be written

$$\Xi_1^{r,t} = \Phi_1 \mathbf{D}_1^{r,t}, \tag{14}$$

where the matrices Ξ_1^r, Ξ_1^t, and ϕ_1 represent the direction cosines of the nine axes in the coordinate systems $OX_1^rY_1^rZ_1^r$, $OX_1^tY_1^tZ_1^t$ and $OX_1^iY_1^iZ_1^i$ in reference to the $OX'Y'Z'$ coordinate system, respectively, and are defined by

$$\Xi_1^{r,t} = \begin{bmatrix} \cos\xi_{x1}^{r,t} & \cos\xi_{y1}^{r,t} & \cos\xi_{z1}^{r,t} \\ \cos\zeta_{x1}^{r,t} & \cos\zeta_{y1}^{r,t} & \cos\zeta_{z1}^{r,t} \\ \cos\eta_{x1}^{r,t} & \cos\eta_{y1}^{r,t} & \cos\eta_{z1}^{r,t} \end{bmatrix}, \tag{15}$$

$$\Phi_1 = \begin{bmatrix} \cos\phi_1^i & -\sin\phi_1^i & 0 \\ \sin\phi_1^i & \cos\phi_1^i & 0 \\ 0 & 0 & 1 \end{bmatrix}. \tag{16}$$

The matrices $\mathbf{D}_1^r$ and $\mathbf{D}_1^t$ denote the direction cosines of the coordinate systems $OX_1^rY_1^rZ_1^r$ and $OX_1^tY_1^tZ_1^t$ in reference to $OX_1^iY_1^iZ_1^i$, respectively, and are defined by

$$\mathbf{D}_1^r = \begin{bmatrix} \cos2\tau_1^i & 0 & \sin2\tau_1^i \\ 0 & -1 & 0 \\ \sin2\tau_1^i & 0 & -\cos2\tau_1^i \end{bmatrix}, \tag{17}$$

$$\mathbf{D}_1^t = \begin{bmatrix} \cos(\tau_1^i - \tau_1^t) & 0 & -\sin(\tau_1^i - \tau_1^t) \\ 0 & 1 & 0 \\ \sin(\tau_1^i - \tau_1^t) & 0 & \cos(\tau_1^i - \tau_1^t) \end{bmatrix}. \tag{18}$$

In these matrices, the elements $\cos\xi_{x1}^r$, $\cos\zeta_{x1}^r$, $\cos\eta_{x1}^r$, $\cos\xi_{y1}^r$, $\cos\zeta_{y1}^r$, and $\cos\eta_{y1}^r$ represent the direction cosines of the first reflected field in relation to $OX'Y'Z'$, respectively. $\cos\xi_{z1}^r$, $\cos\zeta_{z1}^r$, and $\cos\eta_{z1}^r$ are the direction cosines of the ray. The cosine notations with the superscript t are the corresponding quantities for refraction.

C. Two Refractions and Internal Reflections

The refracted ray proceeds into the ice crystal and will hit another hexagonal surface. Consequently internal reflections and additional refractions will take place. The major difference between treatment of internal reflections and refractions and the previous analyses is due to the possible existence of the total internal reflection when the incident angles become larger than a certain critical angle. Assume that a ray inside the crystal hits the next surface at point $N_n(x_n, y_n, z_n)$. Let $\mathbf{n}_n$ denote the normal to the surface whose direction cosines $\cos\alpha_n$, $\cos\beta_n$, and $\cos\gamma_n$ are given by Eqs. (3) or (4). Thus the new incident plane defined by $QTRPSQ$ in Fig. 2(b) can be constructed. As before, three new coordinate systems involving the new incident, reflection, and refraction rays $OX_n^iY_n^iZ_n^i$, $OX_n^rY_n^rZ_n^r$, and $OX_n^tY_n^tZ_n^t$ may be defined. Again it is noted here that the positive direction of the axis OX_n^i is chosen so that the angle between the axis and $\mathbf{n}_n$ is <180° [see Fig. 2(b), the arc RP <180°].

General mathematical expressions for electric fields involving both the amplitude and phase and the traveling directions of the rays may be formulated based on previous analyses. Let the subscript n denote the number of reflections or refractions ($n = 2$, two refractions, $n \geq 3$, internal reflections). For the reflected and refracted electric fields using Fresnel formulas we have

$$\mathbf{E}_n^r = \mathbf{R}_n \mathbf{E}_n^i \qquad \mathbf{E}_n^t = \mathbf{T}_n \mathbf{E}_n^i, \tag{19}$$

where

$$\mathbf{E}_n^i = \begin{bmatrix} E_{xn}^i \\ E_{yn}^i \end{bmatrix} = \begin{cases} \mathbf{P}_2 \mathbf{E}_1^t, & n = 2, \\ \mathbf{P}_{n-1} \mathbf{E}_{n-1}^r, & n \geq 3, \end{cases} \tag{20}$$

$$\mathbf{E}_n^r = \begin{bmatrix} E_{xn}^r \\ E_{yn}^r \end{bmatrix}, \qquad \mathbf{E}_n^t = \begin{bmatrix} E_{xn}^t \\ E_{yn}^t \end{bmatrix}, \qquad n \geq 2, \tag{21}$$

where (E_{xn}^i, E_{yn}^i) represent the electric fields of the incident rays, and (E_{xn}^r, E_{yn}^r) and (E_{xn}^t, E_{yn}^t) are the corresponding electric fields for the reflected and refracted rays on and perpendicular to the incident plane, respectively. The matrix $\mathbf{P}_n$, which represents the necessary coordinate rotation from the incoming refracted ray coordinate system $OX_1^tY_1^tZ_1^t$ (for $n = 2$) or internal reflected ray coordinate system $OX_{n-1}^rY_{n-1}^rZ_{n-1}^r$ (for $n \geq 3$) to $OX_n^iY_n^iZ_n^i$, is given by

$$\mathbf{P}_n = \begin{bmatrix} \cos\phi_n^i & \sin\phi_n^i \\ -\sin\phi_n^i & \cos\phi_n^i \end{bmatrix}, \qquad n \geq 2, \tag{22}$$

where ϕ_n^i is the angle between the axes OX_1^t and OX_2^i (when $n = 2$) or between the axes OX_{n-1}^r and OX_n^i (when $n \geq 3$) and is given by

$$\cos\phi_n^i = \frac{\cos\chi_n}{\sin\omega_n}, \qquad \sin\phi_n^i = \frac{\cos\psi_n}{\sin\omega_n}. \tag{23}$$

In this equation, $\cos\chi_n$, $\cos\psi_n$, and $\cos\omega_n$ are the direction cosines of the normal $\mathbf{n}_n$ with respect to $OX_1^tY_1^tZ_1^t$ (for $n = 2$) or with respect to $OX_{n-1}^rY_{n-1}^rZ_{n-1}^r$ (for $n \geq 3$). In Fig. 2(b) χ_n and ω_n are arcs UR and RT, respectively, and ψ_n is not shown in the figure. Once the direction cosines of $\mathbf{n}_n$ in the $OXYZ$ coordinate are known, its direction cosines $\cos\chi_n$, $\cos\psi_n$, and $\cos\omega_n$ may be obtained through a coordinate transformation as follows:

$$\begin{bmatrix} \cos\chi_n \\ \cos\psi_n \\ \cos\omega_n \end{bmatrix} = \Phi_1 \mathbf{D}_1^t \Phi_2 \mathbf{D}_2^r \ldots \Phi_{n-1} \mathbf{D}_{n-1}^r \mathbf{A} \begin{bmatrix} \cos\alpha_n \\ \cos\beta_n \\ \cos\gamma_n \end{bmatrix}, \qquad n \geq 2, \tag{24}$$

where the $\mathbf{A}$ matrix is given in Eq. (6) and Φ_n and $\mathbf{D}_n^r$ ($n \geq 2$), which represent the coordinate transformation between $OX^i_nY^i_nZ^i_n$ and $OX^t_{n-1}Y^t_{n-1}Z^t_{n-1}$ (or $OX^r_{n-1}Y^r_{n-1}Z^r_{n-1}$) and $OX^r_nY^r_nZ^r_n$ and $OX^i_nY^i_nZ^i_n$, respectively, are determined by

$$\mathbf{\Phi}_n = \begin{bmatrix} \cos\phi^i_n & -\sin\phi^i_n & 0 \\ \sin\phi^i_n & \cos\phi^i_n & 0 \\ 0 & 0 & 1 \end{bmatrix}, \quad n \geq 2, \tag{25}$$

$$\mathbf{D}^r_n = \begin{bmatrix} \cos 2\tau^i_n & 0 & -\sin 2\tau^i_n \\ 0 & -1 & 0 \\ -\sin 2\tau^i_n & 0 & -\cos 2\tau^i_n \end{bmatrix}, \quad n \geq 2, \tag{26}$$

where τ^i_n is the incident angle. When τ^i_n is less than a certain critical value, i.e., $m \sin\tau^i_n \leq 1$, the refracted angle τ^t_n can be determined by

$$\cos\tau^i_n = \cos\omega_n, \qquad \sin\tau^t_n = m \sin\tau^i_n. \tag{27}$$

In Eq. (19) the matrices $\mathbf{R}_n$ and $\mathbf{T}_n$ are given in Eq. (11), except subscript 1 is changed to n and their expressions are described in Eq. (12), but m_1 and m_2 now represent the refractive indices of ice and air, respectively. However, when the incident angle is such that $m \sin^i_n > 1$, total internal reflection takes place, and the Fresnel coefficients are given by[6]

$$R_{x_n} = -\frac{\cos\tau^i_n/m + j(m^2 \sin^2\tau^i_n - 1)^{1/2}}{\cos\tau^i_n/m - j(m^2 \sin^2\tau^i_n - 1)^{1/2}},$$

$$R_{y_n} = -\frac{m \cos\tau^i_n + j(m^2 \sin^2\tau^i_n - 1)^{1/2}}{m \cos\tau^i_n - j(m^2 \sin\tau^i_n - 1)^{1/2}}, \tag{28}$$

and $T_{x_n} = T_{y_n} = 0$. Note that $j = \sqrt{-1}$. The directions of the electric fields and the ray in this case may be obtained based on their direction cosines with respect to $OX'Y'Z'$, which may be expressed in a matrix form:

$$\Xi^{r,t}_n = \mathbf{\Phi}_1\mathbf{D}^r_1\mathbf{\Phi}_2\mathbf{D}^r_2 \ldots \mathbf{\Phi}_{n-1}\mathbf{D}^r_{n-1}\mathbf{\Phi}_n\mathbf{D}^{r,t}_n, \tag{29}$$

where $\Xi^{r,t}_n$ represents the direction cosine matrices of the reflected and refracted electric fields and rays in the $OX'Y'Z'$ coordinate, and $\mathbf{D}^t_n$ is a matrix for transformation of the $OX^t_nY^t_nZ^t_n$ coordinate to the $OX^i_nY^i_nZ^i_n$ coordinate. They are given by

$$\Xi^{r,t}_n = \begin{bmatrix} \cos\xi^{r,t}_{xn} & \cos\xi^{r,t}_{yn} & \cos\xi^{r,t}_{zn} \\ \cos\zeta^{r,t}_{xn} & \cos\zeta^{r,t}_{yn} & \cos\zeta^{r,t}_{zn} \\ \cos\eta^{r,t}_{xn} & \cos\eta^{r,t}_{yn} & \cos\eta^{r,t}_{zn} \end{bmatrix}, \tag{30}$$

$$\mathbf{D}^t_n = \begin{bmatrix} \cos(\tau^t_n - \tau^i_n) & 0 & -\sin(\tau^t_n - \tau^i_n) \\ 0 & 1 & 0 \\ \sin(\tau^t_n - \tau^i_n) & 0 & \cos(\tau^t_n - \tau^i_n) \end{bmatrix}. \tag{31}$$

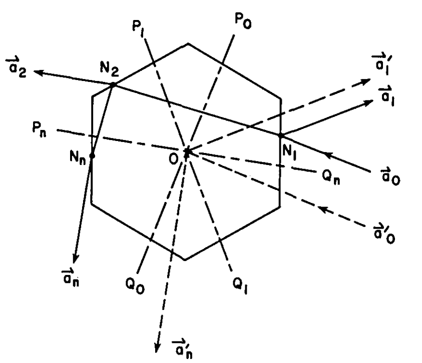

Fig. 3. Geometry of the phase shift of the rays undergoing external reflection $\mathbf{a}_1$, two refractions $\mathbf{a}_2$, and internal reflection $\mathbf{a}_n$. P_0Q_0, P_1Q_1, and P_nQ_n denote planes normal to the direction of these rays.

So far we have derived a number of mathematical expressions governing the electric fields and the outgoing rays relative to the coordinate system $OX'Y'Z'$ defined previously. Now we need to transform the electric vectors due to reflection and refraction events to the scattering plane containing the incident and outgoing rays. Let $E^s_{l_n}$ and $E^s_{r_n}$ be the electric field vector parallel and perpendicular to the scattering plane, respectively, for the externally reflected ($n = 1$) and nth refracted ($n \geq 2$) ray, and let θ_n and ϕ_n ($n = 1, 2, \ldots$) denote the corresponding polar and azimuthal angles with respect to the coordinate system $OX'Y'Z'$. Thus by rotating the direction cosines matrix for the externally reflected and nth refracted outgoing ray in the X' and Y' directions to the plane containing θ_n and ϕ_n, we obtain

$$\mathbf{E}^s_1 = (\mathbf{S}_1\mathbf{N}_1)\mathbf{E}^r_1, \qquad \mathbf{E}^s_n = (\mathbf{S}_n\mathbf{N}_n)E^t_n, \qquad n \geq 2, \tag{32}$$

where

$$\mathbf{E}^s_n = \begin{bmatrix} E^s_{l_n} \\ E^s_{r_n} \end{bmatrix}, \qquad n = 1, 2, \ldots, \tag{33}$$

$$\mathbf{S}_n = \begin{bmatrix} \cos\theta_n \cos\phi_n & \cos\theta_n \sin\phi_n & -\sin\theta_n \\ \sin\phi_n & -\cos\phi_n & 0 \end{bmatrix}, \qquad n = 1, 2, \ldots, \tag{34}$$

$$\mathbf{N}_1 = \begin{bmatrix} \cos\xi^r_{x1} & \cos\xi^r_{y1} \\ \cos\zeta^r_{x1} & \cos\zeta^r_{y1} \\ \cos\eta^r_{x1} & \cos\eta^r_{y1} \end{bmatrix}, \qquad \mathbf{N}_n = \begin{bmatrix} \cos\xi^t_{xn} & \cos\xi^t_{yn} \\ \cos\zeta^t_{xn} & \cos\zeta^t_{yn} \\ \cos\eta^t_{xn} & \cos\eta^t_{yn} \end{bmatrix}, \qquad n \geq 2, \tag{35}$$

$$\theta_1 = \eta^r_{z1}, \qquad \cos\phi_1 = \frac{\cos\xi^r_{z1}}{\sin\eta^r_{z1}}, \qquad \sin\phi_1 = \frac{\cos\zeta^r_{z1}}{\sin\eta^r_{z1}}, \tag{36}$$

$$\theta_n = \eta^t_{zn}, \qquad \cos\phi_n = \frac{\cos\xi^t_{zn}}{\sin\eta^t_{zn}}, \qquad \sin\phi_n = \frac{\cos\zeta^t_{zn}}{\sin\eta^t_{zn}}, \qquad n \geq 2. \tag{37}$$

All notations in these equations have been previously defined.

D. Phase Shift and the Total Electric Field Vector

In the foregoing sections, we have shown that the amplitude and phase as well as the direction of the electric fields of the rays vary due to reflection and refraction events. Moreover the optical path lengths of the rays also lead to changes in the phase of the electric field. Because the incident rays which hit the ice surface at different positions will experience different optical path lengths in or outside the ice crystal, these phase shifts will produce changes in the phase of the outgoing rays.

As shown in Fig. 3, assume that an incident ray $\mathbf{a}_0$ hits the ice surface at the point N_1. The outgoing rays $\mathbf{a}_1$, $\mathbf{a}_2$, and $\mathbf{a}_n$ are successively produced by the external reflection, two refractions, and internal reflections. Through the center point O, we may construct four planes P_0Q_0, P_1Q_1, P_2Q_2, and P_nQ_n perpendicular to the rays $\mathbf{a}_0$, $\mathbf{a}_1$, $\mathbf{a}_2$, and $\mathbf{a}_n$, respectively. Now imagine that there are rays $\mathbf{a}_0'$, $\mathbf{a}_1'$, $\mathbf{a}_2'$, and $\mathbf{a}_n'$ traveling in the space through point O without the existence of the ice crystal and assume that they are parallel to $\mathbf{a}_0$, $\mathbf{a}_1$, $\mathbf{a}_2$, and $\mathbf{a}_n$, respectively. Thus the phase shift of the outgoing ray

$\mathbf{a}_1$ from the imaginary ray $\mathbf{a}_1'$ is determined by the distances between point N_1 and planes P_0Q_0 and P_1Q_1. In reference to the geometry, the distance between N_1 and P_0Q_0 is given by

$$d_0 = |x_1 \cos\alpha_{31} + y_1 \cos\alpha_{32} + z_1 \cos\alpha_{33}|, \tag{38}$$

where x_1, y_1, and z_1 are the three coordinates of point N_1 with respect to the $OXYZ$ coordinate system. Likewise the distance between N_1 and P_1Q_1 is

$$d_1 = |x_1 \cos\alpha_{z1}^r + y_1 \cos\beta_{z1}^r + z_1 \cos\gamma_{z1}^r|, \tag{39}$$

where $\cos\alpha_{z1}^r$, $\cos\beta_{z1}^r$, and $\cos\gamma_{z1}^r$ are the three direction cosines of the ray $\mathbf{a}_1$. They may be derived from coordinate transformation as follows:

$$\begin{bmatrix} \cos\alpha_{z1}^r \\ \cos\beta_{z1}^r \\ \cos\gamma_{z1}^r \end{bmatrix} = \mathbf{A}^* \begin{bmatrix} \cos\xi_{z1}^r \\ \cos\zeta_{z1}^r \\ \cos\eta_{z1}^r \end{bmatrix}, \tag{40}$$

where $\mathbf{A}^*$ is the transpose of the matrix defined in Eq. (6). Thus the phase shift of the ray $\mathbf{a}_1$ from $\mathbf{a}_1'$ may be written

$$\Delta\phi_1 = -\frac{2\pi}{\lambda}(d_0 + d_1), \tag{41}$$

where λ is the wavelength of the light beam.

To find the phase shift of the nth outgoing ray, we define the reflection points N_{n-1} and N_n on the surface of the crystal. Analogous to the discussions above, the path length of $N_{n-1}N_n$ is given by

$$d_{n,n-1} = [(x_n - x_{n-1})^2 + (y_n - y_{n-1})^2 + (z_n - z_{n-1})^2]^{1/2}, \tag{42}$$

and the distance between N_n and P_nQ_n is

$$d_n = |x_n \cos\alpha_{zn}^t + y_n \cos\beta_{zn}^t + z_n \cos\gamma_{zn}^t|, \tag{43}$$

where

$$\begin{bmatrix} \cos\alpha_{zn}^t \\ \cos\beta_{zn}^t \\ \cos\gamma_{zn}^t \end{bmatrix} = \mathbf{A}^* \begin{bmatrix} \cos\xi_{zn}^t \\ \cos\zeta_{zn}^t \\ \cos\eta_{zn}^t \end{bmatrix}. \tag{44}$$

Thus the phase shift of the nth ray $\mathbf{a}_n$ leaving the ice crystal with respect to the ray $\mathbf{a}_n'$ may be written

$$\Delta\phi_n = -\frac{2\pi}{\lambda}[d_0 + d_n - m(d_{21} + d_{32} + \ldots + d_{n,n-1})], \tag{45}$$

where m is the complex refractive index of ice relative to air.

The total electric field vector, including the amplitude and phase for all incident rays which undergo external reflection, two refractions, and internal reflection, may be obtained by summing the outgoing electric field vectors having the same direction in space as follows:

$$\mathbf{E}^s(\theta,\phi) = \sum_q \left\{ \sum_n \delta(\theta_n - \theta, \phi - \phi_n) w_n \mathbf{E}_n^s(\theta_n,\phi_n) \times \exp\left[-jk\left(d_0 + d_n - m\sum_{l=1}^{n} d_{l+1,l}\right)\right]\right\}_q, \tag{46}$$

where q denotes the number of the incident rays used, the δ-function

$$\delta(\theta - \theta_n, \phi - \phi_n) = \begin{cases} 1, \text{ when } \theta = \theta_n,\ \phi = \phi_n, \\ 0, \text{ otherwise}, \end{cases} \tag{47}$$

and the weight of the electric field for oblique incident rays may be derived on the basis of the energy conservation principle and is given by

$$w_n^2 = \begin{cases} 1, & n = 1, \\ \dfrac{\cos\tau_n^t \cos\tau_1^t}{\cos\tau_n^i \cos\tau_1^i} \dfrac{m_r^2}{m_r^2 + m_i^2}, & n \geq 2. \end{cases} \tag{48}$$

When $m_i = 0$, w_n^2 reduces to the form given in Born and Wolf[7] (p. 41).

III. Diffraction

In the limit of Fraunhofer diffraction for the far field, the wave disturbance of the light beam at an arbitrary point P may be expressed by[8]

$$u_p = -\frac{ju_0}{\lambda r} \iint_{B'} \exp(-jkr)dx'dy', \tag{49}$$

where u_0 represents the disturbance in the original wave at point O on the plane wave front with wavelength λ, r is the distance between point P and point $O'(X',Y')$ on the aperture with an area B' and $k = 2\pi/\lambda$. The eight apexes B_i' (i = 1–8) shown in Fig. 4 are the projections of the eight vertices B_i (i = 1–8) of the hexagonal crystal on the plane perpendicular to an oblique incident light ray. The coordinates of the eight vertices as set up in Fig. 1 are given by $B_1(O,a,L/2)$, $B_2(-\sqrt{3}a/2,a/2,L/2)$, $B_3(-\sqrt{3}a/2,-a/2,L/2)$, $B_4(O,-a,L/2)$, $B_5(O,-a,-L/2)$, $B_6(\sqrt{3}a/2,-a/2,-L/2)$, $B_7(\sqrt{3}a/2,a/2,-L/2)$, and $B_8(O,a,-L/2)$. Their projections on the aperture plane normal to the incident ray in the $OX'Y'Z'$ system (i.e., $X'Y'$ plane) may be obtained through a coordinate transformation as follows:

$$\begin{bmatrix} x'_{B_i} \\ y'_{B_i} \end{bmatrix} = \begin{bmatrix} \cos\alpha_{11} & \cos\alpha_{12} & \cos\alpha_{13} \\ \cos\alpha_{21} & \cos\alpha_{22} & \cos\alpha_{23} \end{bmatrix} \begin{bmatrix} x_{B_i} \\ y_{B_i} \\ z_{B_i} \end{bmatrix}. \tag{50}$$

Let θ_p and ϕ_p be the polar and azimuthal angles of the diffracted light beam with respect to the $OX'Y'Z'$ system. Then Eq. (49) may be integrated to give

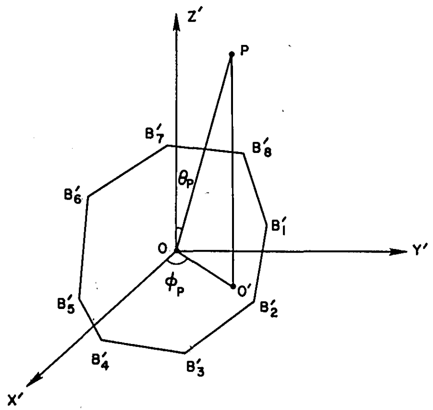

Fig. 4. Geometry for Fraunhofer diffraction at an arbitrary point p. B_i' (i = 1–8) are the projections of the eight vertices of a hexagonal crystal on the plane normal to an oblique incident ray. θ_p and ϕ_p are the polar and azimuthal angles of the diffracted light beam with respect to the $OX'Y'Z'$ system.

$$u_p(\theta_p,\phi_p) = -\frac{ju_0}{\lambda r}\iint_{B'} \exp[-jk(x'\cos\phi_p + y'\sin\phi_p)\sin\theta_p dx'dy']$$
$$= -\frac{ju_0}{k^2\lambda r}\sum_{i=1}^{8}\left(\frac{g_i}{P_iC_i} - \frac{h_i}{P_iD_i}\right), \quad (51)$$

where

$$C_i = q_i + P_i a_{i+1}, \qquad D_i = q_i + P_i b_i,$$
$$g_i = \exp(-jkD_i v_{i+1}) - 1,$$
$$h_i = \exp(-jkP_i u_i)[\exp(-jkC_i v_{i+1}) - 1],$$
$$P_i = \sin\theta_p \cos(\phi_p - \psi_i), \qquad q_i = \sin\theta_p \sin(\phi_p - \psi_i),$$
$$\tan\psi_i = y'_{B_i}/x'_{B_i},$$
$$u_i = x'_{B'_i}\cos\psi_i + y'_{B'_i}\sin\psi_i,$$
$$v_i = -x'_{B'_i}\sin\psi_i + y'_{B'_i}\cos\psi_i,$$
$$a_i = u_i/v_i, \qquad b_i = (u_{i+1} - u_i)/v_{i+1}, \qquad i = 1,2,\ldots,7.$$

For $i = 8$, we should have $a_{i+1} = a_1$, $b_i = (u_1 - u_8)/v_1$, $u_{i+1} = u_1$, and $v_{i+1} = v_1$. When $\theta_p = \phi_p = 0$, we find from Born and Wolf[7] (p. 386) that

$$u_p(0,0) = -\frac{ju_0}{\lambda r}\iint_{B'} dx'dy'$$
$$= -\frac{ju_0}{2\lambda r}\Big[(x'_{B'_8}y'_{B'_1} - x'_{B'_1}y'_{B'_8}) + \sum_{i=1}^{7}(x'_{B'_i}y'_{B'_{i+1}} - x'_{B'_{i+1}}y'_{B'_i})\Big]. \quad (52)$$

Let the incident electric fields be denoted as $E_{x'0}$ and $E_{y'0}$; then the diffracted electric fields on the $OX'Y'Z'$ system are given by

$$\mathbf{E}^{f'} = \begin{bmatrix} E^f_{x'} \\ E^f_{y'} \end{bmatrix} = u_p(\theta_p,\phi_p)\begin{bmatrix} E_{x'0} \\ E_{y'0} \end{bmatrix}. \quad (53)$$

As before, the two components of electric fields of diffraction with respect to the scattering plane can be obtained through a coordinate transformation as follows:

$$\mathbf{E}^f = u_p \mathbf{S}^f \begin{bmatrix} E_{x'0} \\ E_{y'0} \end{bmatrix}, \quad (54)$$

where the transformation matrix is

$$\mathbf{S}^f = \begin{bmatrix} \cos\theta_p\cos\phi_p & \cos\theta_p\sin\phi_p \\ \sin\phi_p & -\cos\phi_p \end{bmatrix}, \quad (55)$$

the electric fields parallel and perpendicular to the scattering plane are

$$\mathbf{E}^f = \begin{bmatrix} E^f_l \\ E^f_r \end{bmatrix}. \quad (56)$$

IV. Scattering Phase Matrix for Randomly Oriented Ice Crystals

The electric field vectors for the geometric reflection, refraction, and diffraction have been derived in Secs. II and III, respectively. In this section we wish to derive the relevant equations for computations of the scattering phase matrix for randomly oriented ice crystals. According to the coordinate systems described previously, we may express the scattered electric field for a hexagonal ice crystal in the form[9]

$$\begin{bmatrix} E_l \\ E_r \end{bmatrix}_{Z'OP} = \begin{bmatrix} A_2 & A_3 \\ A_4 & A_1 \end{bmatrix}\begin{bmatrix} E_{x'0} \\ E_{y'0} \end{bmatrix}_{Z'OX'}, \quad (57)$$

where E_l and E_r represent the parallel and perpendicular components of the scattered electric field, respectively, with respect to the scattering plane $Z'OP$, and $E_{x'0}$ and $E_{y'0}$ are those of the incident electric field with respect to the incidence plane $Z'OX'$ as shown in Fig. 5. Based on the analyses given in Secs. II and III, the amplitude functions A_1, A_2, A_3, and A_4 defined in Eq. (57) may be written

$$\mathbf{A} = \mathbf{A}^f + \mathbf{A}^s = \begin{bmatrix} A^f_2 & A^f_3 \\ A^f_4 & A^f_1 \end{bmatrix} + \begin{bmatrix} A^s_2 & A^s_3 \\ A^s_4 & A^s_1 \end{bmatrix}, \quad (58)$$

where

$$\mathbf{A}^f = u_p r \mathbf{s}^f, \quad (59)$$
$$\mathbf{A}^s = \sum_q \left\{\sum_n \delta(\theta - \theta_n; \phi - \phi_n) w_n \mathbf{C}^s_n(\theta_n,\phi_n) \times \exp\left[-jk\left(d_0 + d_n - m\sum_{l=1}^{n} d_{l+1,l}\right)\right]\right\}_q, \quad (60)$$

$$\left.\begin{aligned} \mathbf{C}^s_1 &= (\mathbf{S}_1\mathbf{N}_1)\mathbf{R}_1\mathbf{P}_1, \\ \mathbf{C}^s_2 &= (\mathbf{S}_2\mathbf{N}_2)\mathbf{T}_2\mathbf{P}_2\mathbf{T}_1\mathbf{P}_1, \\ &\;\;\vdots \\ \mathbf{C}^s_n &= (\mathbf{S}_n\mathbf{N}_n)\mathbf{T}_n\mathbf{P}_n\mathbf{R}_{n-1}\mathbf{P}_{n-1}\mathbf{R}_{n-2}\mathbf{P}_{n-2}\ldots\mathbf{R}_2\mathbf{P}_2\mathbf{T}_1\mathbf{P}_1. \end{aligned}\right\} \quad (61)$$

The Stokes parameters of the scattered light are now given by

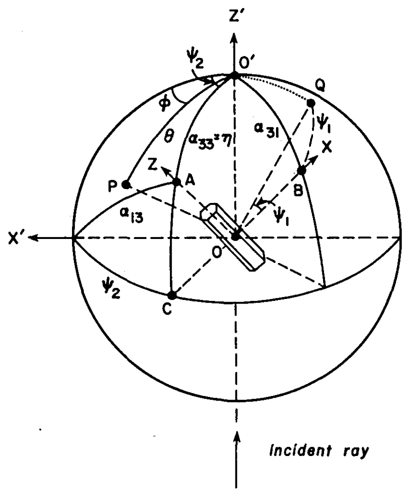

Fig. 5. Geometry of the scattering by an arbitrarily oriented hexagon in space. The scattering plane is described by $Z'OP$. The incident ray plane is defined by $Z'OX'$. θ and ϕ are the scattering and azimuthal angles for the scattered rays at an arbitrary point P. $\cos\alpha_{31}$, $\cos\alpha_{33}$, and $\cos\alpha_{13}$ are the direction cosines between the axes OZ' and OX, OZ' and OZ, and OX' and OZ, respectively. $\eta(=\alpha_{33})$ and ψ_2 are orientation angles of the long axis of the crystal (Z axes) with respect to the zenith (OZ') and azimuthal (OX') directions. ψ_1 is also an orientation angle which is an angle between the normal to the crystal surface (OX) and OQ, where Q is the intersection of the arc $CAO'Q$ on the sphere with the normal plane (XY). ψ_1 varies from 0 to 2π, but because of the hexagonal symmetry it changes only from 0 to $\pi/3$.

$$\begin{bmatrix} I \\ Q \\ U \\ V \end{bmatrix} = \mathbf{F}(\theta,\phi) \begin{bmatrix} I_0 \\ Q_0 \\ U_0 \\ V_0 \end{bmatrix}, \quad (62)$$

where the general transformation matrix is

$$\mathbf{F} = \begin{bmatrix} \tfrac{1}{2}(M_2 + M_3 + M_4 + M_1) & \tfrac{1}{2}(M_2 - M_3 + M_4 - M_1) & S_{23} + S_{41} & D_{23} + D_{41} \\ \tfrac{1}{2}(M_2 + M_3 - M_4 - M_1) & \tfrac{1}{2}(M_2 - M_3 - M_4 + M_1) & S_{23} - S_{41} & D_{23} - D_{41} \\ S_{24} + S_{31} & S_{24} - S_{31} & S_{21} + S_{34} & D_{21} - D_{34} \\ D_{24} + D_{13} & D_{42} - D_{13} & D_{12} + D_{43} & S_{21} - S_{34} \end{bmatrix}, \quad (63)$$

$$M_k = A_k A_k^* = |A_k|^2,$$

$$S_{kl} = S_{lk} = \tfrac{1}{2}(A_l A_k^* + A_k A_l^*),$$

$$-D_{kl} = D_{lk} = \frac{j}{2}(A_l A_k^* - A_k A_l^*), \qquad l,k = 1, 2, 3, 4.$$

The scattering phase matrix $\mathbf{P}$ is defined by

$$\mathbf{P} = C\mathbf{F}, \quad (64)$$

where $C = 4\pi/\sigma_s$, and the scattering cross section

$$\sigma_s = \int_0^{2\pi} \int_0^{\pi} (E_l E_l^* + E_r E_r^*) \sin\theta d\theta d\phi. \quad (65)$$

In this case the scattering phase matrix is said to be normalized so that

$$\int_{4\pi} P_{11}(\Omega) d\Omega / 4\pi = 1. \quad (66)$$

In reference to Fig. 5, the scattering phase matrix elements for an arbitrarily oriented hexagonal ice crystal not only depend on the scattering and azimuthal angles with respect to the incident light rays but also depend on the orientation angles of the ice crystal η, ψ_2, and ψ_1 defined in the figure. ψ_1 is the angle denoting the orientation of a hexagonal crystal with respect to its long axis on the XY plane and $\cos\psi_1 = \cos\alpha_{31}/\sin\alpha_{33}$. η is the orientation angle in the zenith direction and $\cos\eta = \cos\alpha_{33}$, the direction cosine between the Z and Z' axis. ψ_2 is the orientation angle in the azimuthal direction and $\cos\psi_2 = \cos\alpha_{13}/\sin\alpha_{33}$. To obtain the scattering phase matrix for randomly oriented hexagonal crystals in 3-D space, an angular integration with respect to ψ_1 is to be performed first as follows:

$$\mathbf{P}(\theta,\phi;\eta,\psi_2) = \frac{1}{2\pi} \int_0^{2\pi} \mathbf{P}(\theta,\phi;\eta,\psi_2,\psi_1) d\psi_1. \quad (67)$$

Since the scattering phase matrix for randomly oriented particles is independent of ϕ, which is in the same azimuthal plane as ψ_2, we obtain

$$\mathbf{P}(\theta) = \frac{1}{4\pi} \int_0^{2\pi} \int_0^{\pi} \mathbf{P}(\theta,0;\eta,\psi_2) \sin\eta d\eta d\psi_2. \quad (68)$$

Moreover for randomly oriented particles, the scattering phase matrix contains only six independent elements in the form

$$\mathbf{P}(\theta) = \begin{bmatrix} P_{11} & P_{12} & 0 & 0 \\ P_{12} & P_{22} & 0 & 0 \\ 0 & 0 & P_{33} & -P_{43} \\ 0 & 0 & P_{43} & P_{44} \end{bmatrix}. \quad (69)$$

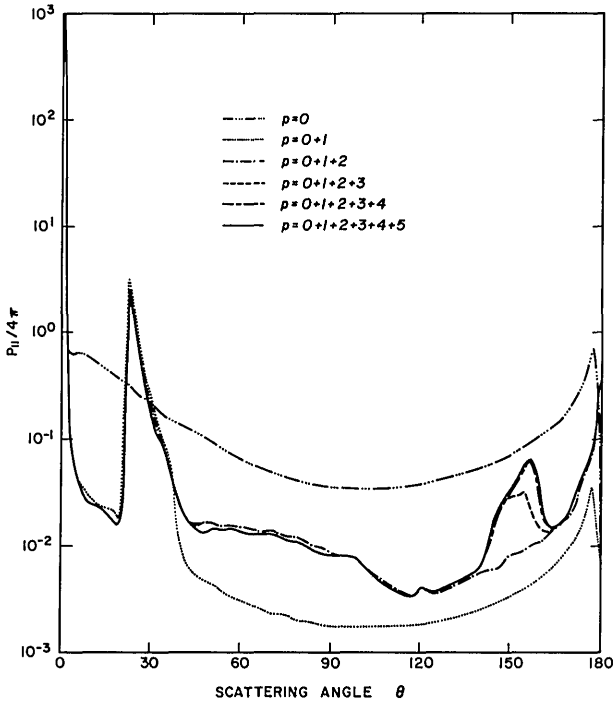

Fig. 6. Contributions of the scattering phase function as a function of the scattering angle for external reflection, two refractions, and internal reflections up to four. The columns with a length-to-radius ratio of 300/60 μm are assumed to be randomly oriented in a horizontal plane when the incident beam with a 0.55-μm wavelength is normal to this plane.

Computational results for these elements based on geometrical ray tracing analyses will be presented in the next section.

V. Computational Results and Discussions

To estimate the required internal reflections in the geometric ray tracing calculations so that energies associated with incoming and outgoing rays are approximately conserved, we first examine the energies for external reflection ($p = 0$), two refractions ($p = 1$), and internal reflections ($p \geq 2$) for randomly oriented column crystals. These crystals have a length-to-radius ratio of 300/60 μm, and an incident light beam with a 0.55-μm wavelength is normal to the crystals. Shown in Fig. 6 are separate normalized phase functions ($P_{11}/4\pi$) for external reflection, and the sums of the individual components and external reflection are also

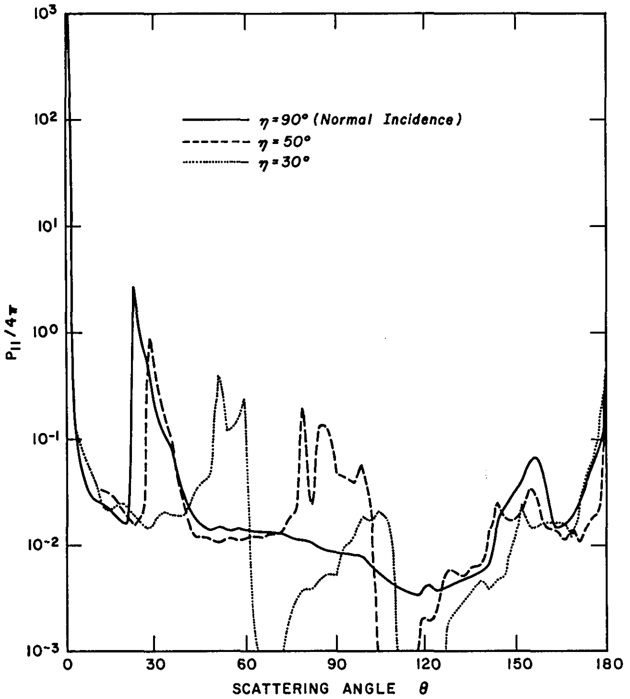

Fig. 7. Averaged scattering phase function as a function of the scattering angle for randomly oriented columns in a horizontal plane when the incident angles are 90 (normal incidence), 50, and 30°.

indicated in the figure. Contributions of the externally reflected rays range over all scattering angles with a small peak near ~175°. The 22° halo maximum is basically produced by two refractions. Energy peaks at an ~160° scattering angle and at backscattering are caused by internal reflections greater than two. External reflection accounts for ~4.2% of the total incident energy. The inclusion of two refractions and one, two, three, and four internal reflections gives, respectively, 85.7, 93.3, 94.8, 96.4, and 97.5% of the total incident energy. For oblique incidence, the percentages of energy distributions are roughly about the same as the above values. In the following presentations, we have included internal reflections up to five.

Figure 7 illustrates the effect of the incident angle η (90° elevation angle) on the scattering phase function. Note that the scattered phase function has been averaged over the azimuthal angle ψ_2 and the rotational angle ψ_1 with respect to the ice crystal axes as presented in Sec. IV. Incident angles of 90 (normal incidence), 50, and 30° are used. For normal incidence, we see a sharp 22° halo peak, a broad maximum at 160°, and a peak in the backscattering direction. For the oblique incident angle of 50°, the scattering pattern becomes much more complex. The halo shifts to a 30° scattering angle. In addition to the halo peak, there are also a number of maxima located at scattering angles of ~70, 85, and 160°. For the oblique incident angle of 30°, the maxima occur at ~50, 100, and 150°. The phase function peaks in the backscattering direction regardless of the direction of the incident light.

Figure 8 shows the degree of linear polarization as a function of the scattering angle for the aforementioned three incident angles when the column crystals are randomly oriented in a horizontal plane. For normal incidence, the most pronounced feature is the positive polarization with a maximum of the order of 75% located at the 120° scattering angle. The pattern is broad and differs from the rainbow features produced by spherical water droplets. The 22° halo shows a negative polarization of the order of 3–8%, which is in agreement with observations presented by Minnaert.[10] On the side of the halo minimum, two maximum polarization patterns are shown. For a 50° oblique incidence, polarization values beyond the 100° scattering angle become very small. The negative polarization for the 22° halo reduces somewhat, and the two polarization maxima become larger than those from normal incidence. When the incident angle is 30°, polarization of the scattered light is quite small, except at the 120° scattering angle where the large positive polarization (~94%) is caused by external reflection. This scattering angle may be thought of as the Brewster angle at which the unpolarized light is totally polarized due to external reflection. The degree of linear polarization for randomly oriented columns in 3-D space will be presented below.

Figure 9 shows six independent elements of the scattering phase matrix for column crystals randomly oriented in 3-D space. Graphs for P_{12}, P_{22}, P_{33}, P_{43}, and P_{44} are plotted relative to the normalized phase function P_{11}. For P_{11}, a strong forward scattering caused by diffraction is seen. In addition the 22 and 46° halos are both shown. The 22° halo is ~1 order of magnitude stronger than the 46° halo. The backscattering peak is also quite pronounced. The minimum scattering pattern is found at ~125°. At 160°, a broad maximum is seen which is produced by internal reflections. This maximum resembles, but is not quite the same as, the rainbow features produced by water spheres. It should be noted that columns with a 300-μm length and a 60-μm radius probably would not be randomly oriented in realistic atmospheres so that some of the scattering features shown in the left-hand side of Figs. 9 and 10 may not be evidenced in the sky.

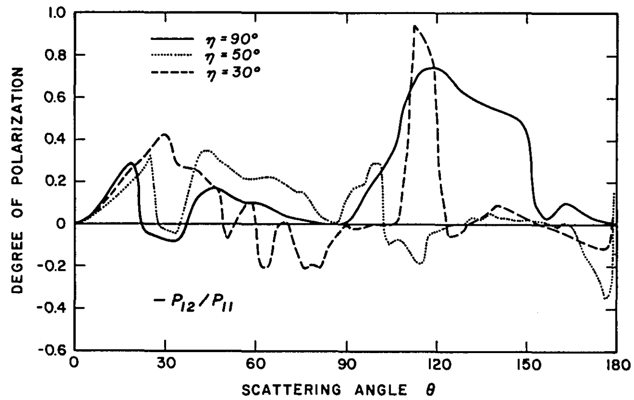

Fig. 8. Averaged degree of linear polarization as a function of the scattering angle for randomly oriented columns in a horizontal plane where the incident angles are 90, 50, and 30°.

Physically $-P_{12}/P_{11}$ ($= -Q/I$) represents the degree of linear polarization when the incident light is unpolarized. This figure shows that polarization values are positive over most of the scattering angle. Negative polarization is shown at angles associated with 22 and 46° halo maxima as well as near backscattering direction. The largest polarization is located at a scattering angle of ~125° with a value of ~35% for randomly oriented columns. The element P_{22}/P_{11} is related to the depolarization of scattering light when the incident light is linearly polarized. It is approximately equal to unity in the forward directions and approaches zero at ~175° scattering angle. Values for P_{43}/P_{11} are generally small and fluctuate around zero. This curve is very similar to results presented by Asano and Sato[11] for a prolate spheroid with a major-to-minor axis ratio of 5 which is the same as the one used in the geometric ray tracing calculation. The only exception is that the present

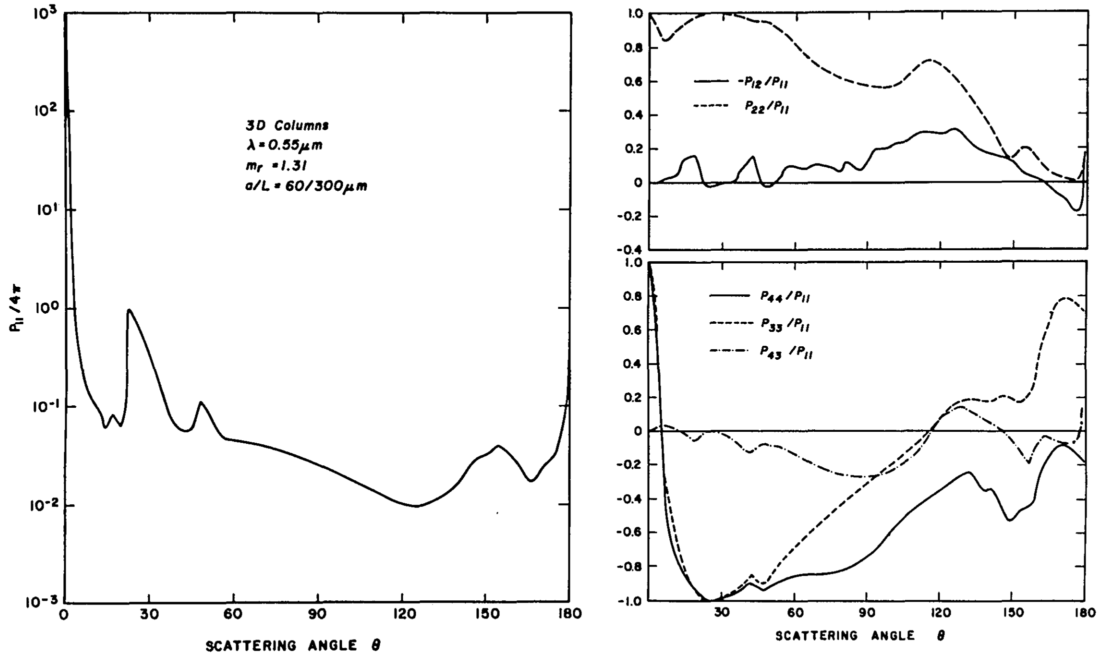

Fig. 9. Angular distribution of six independent elements of the scattering phase matrix for 3-D randomly oriented columns with a length-to-radius of 300/60 μm illuminated by a wavelength of 0.55 μm.

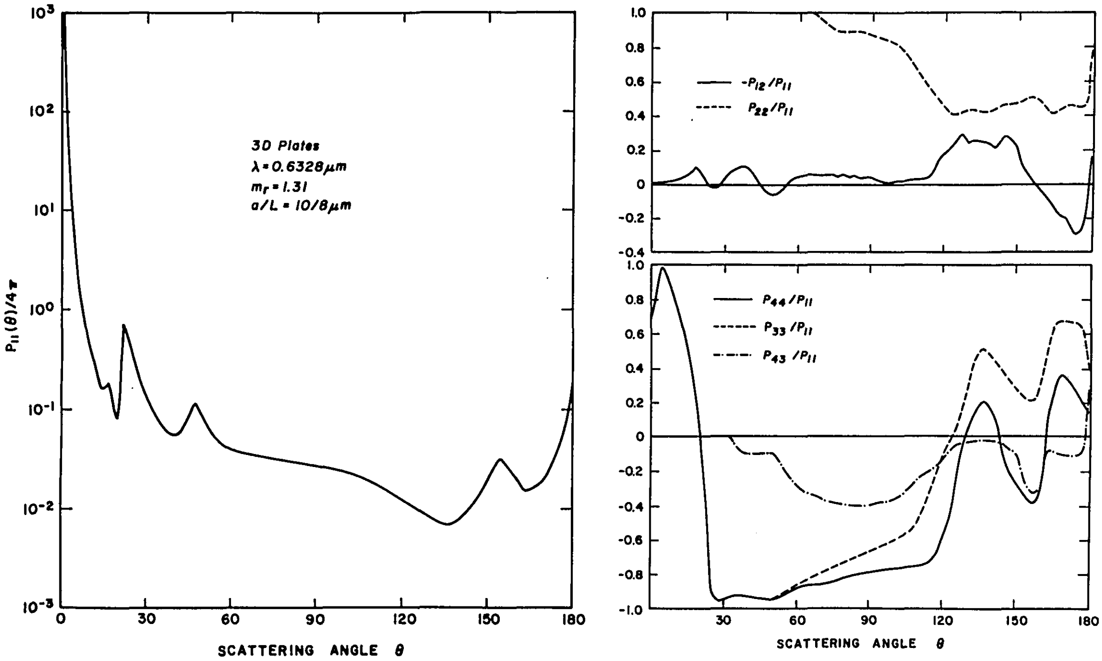

Fig. 10. Angular distribution of six independent elements of the scattering phase matrix for 3-D randomly oriented plates with a length-to-radius ratio of 8/10 μm illuminated by a laser wavelength of 0.6328 μm.

results show positive values for scattering angles from ~120 to 150°. Values for P_{33}/P_{11} and P_{44}/P_{11} are quite different from results presented by Asano and Sato for a prolate spheroid. The P_{44} component may be considered as an expression for the ellipticity of the scattered electric field when the incident light is circularly polarized. Both P_{33}/P_{11} and P_{44}/P_{11} values decrease rapidly from ~1 to −1 when the scattering angle increases from 0 to 20°. Values for P_{33} are usually larger than those for P_{44}. The P_{33} curve shifts from the negative to the positive when the scattering angle is ~120°. However, values for P_{44} remain negative.

In Fig. 10, we show six phase matrix elements for plate crystals having a 10-μm radius and a 8-μm length randomly oriented in space using a 0.6328-μm laser wavelength. Values for P_{22} are the same as those for P_{11} below ~60°. The P_{43} element is negative for small plates except in the backscattering direction, and its values are generally rather small. Values for P_{44}/P_{11} and P_{33}/P_{11} show an increase at a scattering angle of ~10° and then decrease rapidly to the 30° scattering angle region. Both elements show maxima at scattering angles of ~140 and 170°. The patterns of the six phase matrix elements for randomly oriented small plates generally resemble those for randomly oriented large columns. More detailed comparisons of P_{11} and $-P_{12}/P_{11}$ for columns and plates will be given in the following two figures.

In Fig. 11, we compare the computed and measured scattering phase functions P_{11} for randomly oriented columns and plates. The measured scattering phase function is derived from a number of scattering experiments for plates using a 0.6328-μm laser beam described by Sassen and Liou.[4] The dimension of the plates is ~5 μm. In the experiment, the incident laser beam was either horizontally or vertically polarized. In addition to the original components, we also measured the cross-polarized elements. This allows us to construct four phase matrix elements defined in Sec. IV. The vertical bars in this figure and the next figure depict the standard deviation of the measured data as a function of the scattering angle. Large columns generate a larger and broader peak at the 22° halo region and at the 150° scattering angle region. However, the basic features are the same for hexagonal columns and plates. The computed phase function values are in general agreement with experimental data. The experimental data reveal small maxima at ~22 and 155° scattering angles which agree with results derived from geometric ray tracing calculations.

Comparisons of the computed and measured degree of linear polarization and depolarization ratios using a horizontally polarized light for columns and plates are illustrated in the upper and lower diagrams of Fig. 12, respectively. For the degree of linear polarization, there is a general agreement between computed results and experimental data. The computed linear polarization for 20-μm sized plates closely matches the experimental data for plates having a model diameter of ~5 μm, especially at the two maxima in the forward directions and the peaks in the 120–150° scattering region. In the

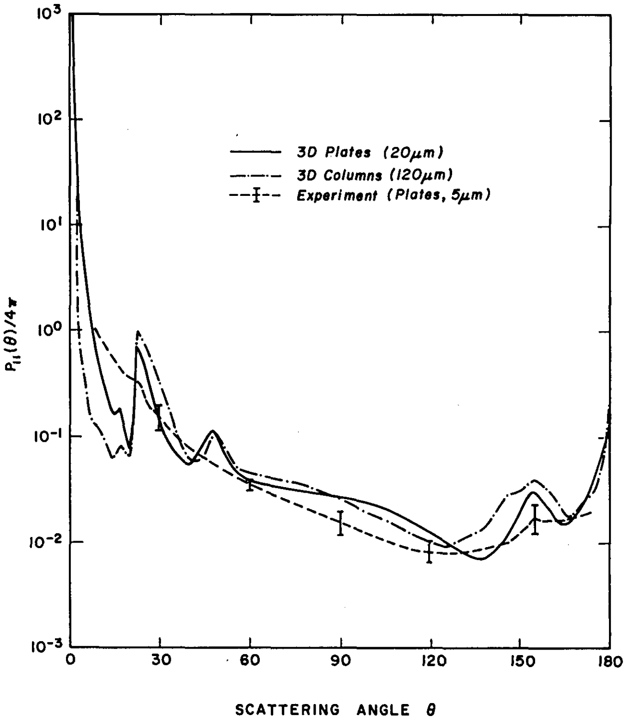

Fig. 11. Comparisons of the computed and measured scattering phase functions for randomly oriented columns and plates. The plates observed in a number of scattering and cloud physics experiments have a modal dimension of ~5 μm.

90–120° scattering region, however, the computed polarization is smaller than the measured values, probably because there might be a number of large columns present during the scattering and cloud physics experiments. In view of the geometric optics approximation used in the theoretical analysis, it is apparent that the agreement between the computed and measured polarization is very good. As for the depolarization ratio, the computed results for 20-μm randomly oriented plates quite closely match the measured data presented by Sassen and Liou.[12] The depolarization ratio in a scattering angle of ~10° shows a maximum of the order of 10% for randomly oriented large columns. Also note that large columns generate ~60% depolarization in the backscattering, while small plates produce a depolarization of ~25%. The backscattering depolarization values shown in this figure and in Fig. 8 are in general agreement with laboratory experimental results presented by Liou and Lahore[13] and Sassen and Liou[12] and with the lidar field data obtained by Sassen[14] for ice clouds.

VI. Conclusion

We have developed a scattering model for arbitrarily oriented hexagonal ice crystals including complete polarization information on the basis of the ray tracing principle. The ray tracing program includes the contribution of the geometric reflection and refraction and the Fraunhofer diffraction. For the geometric optics part, a traceable and analytic procedure was derived for

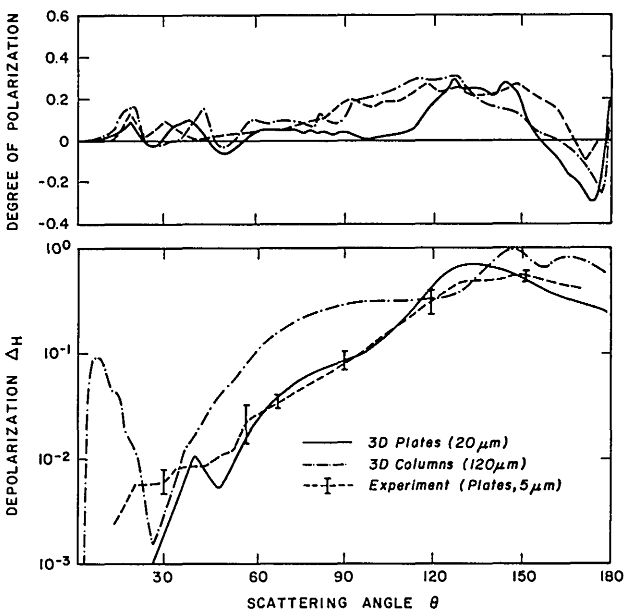

Fig. 12. Comparisons of the computed and measured degree of linear polarization (upper diagram) and depolarization ratio (lower diagram) for randomly oriented columns and plates. The modal dimension of the plates in the scattering experiments is ~5 μm.

computation of scattered energies due to external reflection, two refractions, and internal reflections. From consideration of the direction cosine of the incident electric vector of a ray and the geometry of the hexagonal crystal, consisting of six symmetric and identical sides and top and bottom surfaces, the electric vector of this ray undergoing reflection and refraction can be traced until it emerges out of the crystal. Moreover, the phase shift caused by the different path lengths of a bundle of rays can be included in the analysis to give four complex amplitudes. The diffraction part is determined on the basis of the Fraunhofer limit in the far field in which an analytic expression can be derived for the wave disturbance of light rays produced by an oblique hexagonal aperture. We further developed a theoretical foundation for computation of the scattering phase matrix for randomly oriented hexagonal crystals in 2-D and 3-D space by carrying out proper integrations on the total scattered electric vector with respect to the scattering plane.

Scattered energies associated with external reflection, two refractions, and a number of internal reflections are analyzed, and we show that inclusion of up to five internal reflections gives ~98% of the incident energy for most refractive indices. Results of the phase function and degree of linear polarization for randomly oriented columns in 2-D space are presented for a number of elevation angles. The polarization patterns reveal interesting features in various regions of the scattering angle. Six scattering phase matrix elements for randomly oriented large columns and small plates are illustrated, and their relative magnitudes are discussed. Finally we compare the computed scattering phase function, degree of linear polarization, and depolarization ratio for columns and plates with experimental data measured by Sassen and Liou[4,12] for small plates. We show that the present theoretical results in the limit of the geometric optics principles are in general agreement with laboratory data.

This research was supported by the Air Force Office of Scientific Research under contract F49620-79-C-0198 and in part by the Division of Atmospheric Sciences of the National Science Foundation under grant ATM-81-09050. Q. Cai is on leave from the Lanzhou Institute of Plateau Atmospheric Physics, Academia Sinica, China.

References

1. H. Jacobowitz, J. Quant. Spectrosc. Radiat. Transfer **11**, 691 (1971).
2. K. N. Liou, J. Atmos. Sci. **29**, 524 (1972).
3. P. Wendling, R. Wendling, and H. K. Weickmann, Appl. Opt. **18**, 2663 (1979).
4. K. Sassen and K. N. Liou, J. Atmos. Sci. **36**, 838 (1979).
5. R. F. Coleman and K. N. Liou, J. Atmos. Sci. **38**, 1260 (1981).
6. D. Clare and J. F. Grainger, *Polarized Light and Optical Measurement* (Pergamon, New York, 1971), p. 56.
7. M. Born and E. Wolf, *Principles of Optics* (Pergamon, New York, 1975), pp. 41, 386.
8. K. N. Liou, *An Introduction to Atmospheric Radiation* (Academic, New York, 1980), p. 146.
9. H. C. van de Hulst, *Light Scattering by Small Particles* (Wiley, New York, 1957), p. 43.
10. M. Minnaert, *The Nature of Light and Color in the Open Air* (Dover, New York, 1954), p. 195.
11. S. Asano and M. Sato, Appl. Opt. **19**, 962 (1980).
12. K. Sassen and K. N. Liou, J. Atmos. Sci. **36**, 852 (1979).
13. K. N. Liou and H. Lahore, J. Appl. Meteorol. **13**, 257 (1974).
14. K. Sassen, J. Appl. Meteorol. **16**, 425 (1977).